Electronic Supplementary Material (ESI) for ChemComm.

Magnetic frustration in the high-pressure Mn_2MnTeO_6 (Mn_3TeO_6–II) double perovskite.

Ángel M. Arévalo-López[a]*, Elena Solana-Madruga,[b] Cintli Aguilar-Maldonado,[a] Clemens Ritter,[c] Olivier Mentré [a] and J. Paul Attfield*[b]

Figure S1 shows the structures for M_3TeO_6 with M = Mn, Co and Ni. The three of them are different, however they are related to the corundum-type structure showing octahedral coordination for both cations.

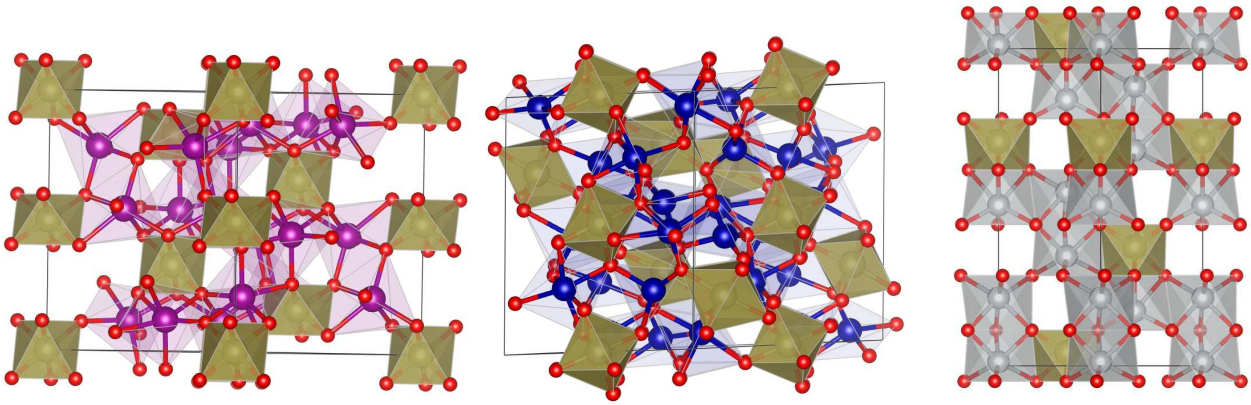

Figure SF1. M_3TeO_6 (M = Mn, Co and Ni) structures with structural parameters: *R*-3, *a* = 8.87 Å, c = 10.67 Å (Mn_3TeO_6) left. *C*2/*c*, *a* = 14.81 Å, *b* = 8.84 Å, *c* = 10.36 Å and *β* = 94.8° (Co_3TeO_6) middle. *R*3, *a* = 5.11 Å, *c* = 13.78 Å (Ni_3TeO_6) right.

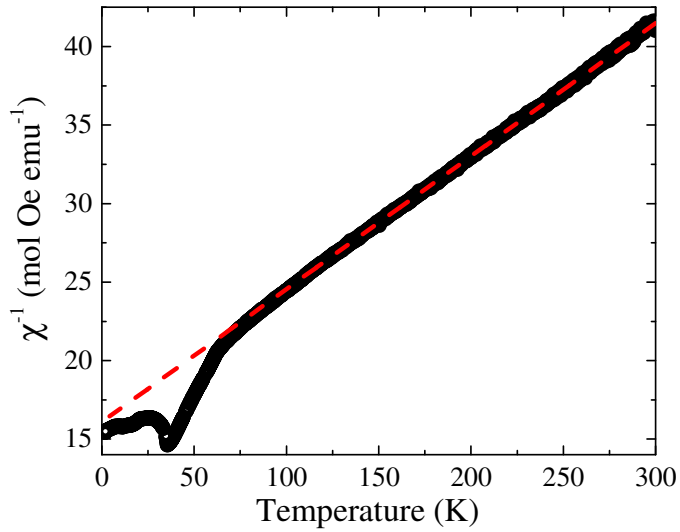

Figure SF2. Inverse magnetic susceptibility showing the complete temperature range. The Curie-Weiss fit between 100 K and 300 K (extrapolated down to 2 K) is depicted with a dashed red line. It results in a μ_{eff} = 5.6 μB/Mn^{2+}, in good agreement with the theoretical value of 5.92μ_B for spin only Mn^{2+} (S=5/2) and a negative Weiss constant of θ= -183(1) K.

Magnetic structure determination:

The magnetic peaks observed at low temperature are indexed with the propagation vector k = [½ 0 ½]. The magnetic symmetry analysis using the BasIreps tool of FullProf Suite[1], results in four possible irreducible representations (Ireps) summarised in Table S1. Ireps 1-4 stand for the possible spin arrangements of Mn_A, while Mn_B (sitting on the two first symmetries) can only follow Ireps Γ_2 and Γ_4, which stand for the AFM (FM) alignment of the magnetic moments along *a* and *c* axis and their FM (AFM) order along *b*. On the other hand, Mn_A would be FM along *b* and *a/c* if following Ireps Γ_1 and Γ_3 respectively.

All simple possible models were tested. The best fit was obtained for both Mn_A and Mn_B following Γ_4 (R_B = 6%, R_f = 5%, R_{Mag} = 7.1%, χ^2 = 1.21 for T = 1.5 K). The magnetic moments can be refined independently, giving maximum values of μ_A = 4.79(6) μ_B and μ_B = 3.8(1) μ_B. In both cases, independent components along *a* and *c* directions could be refined, as shown in Figure SF2. The fit of the complete NPD data set using the magnetic structure model gives the coherent evolution of the magnetic moments with temperature shown in the main text. The fit to the critical law gives their common transition temperature T_N = 35.8(1) K and $\beta \approx 0.2$. The low value of β suggests a 2D XY model. Despite the long-range order observed from magnetic susceptibility and the sharp peaks in the low temperature NPD data, the low dimensionality is supported by the high frustration index obtained from the Curie-Weiss fit to the inverse magnetic susceptibility ($|\theta|/T_N \sim 5$) and the reduced magnetic moment refined for Mn^{2+} at the B sites. For these reasons, a more complex model of the magnetic structure is considered here attending to the main interatomic distances and angles.

Figures SF3a and SF3b show a detailed view of the proposed 2D magnetic structure. The *ac* plane of the nuclear unit cell is marked with a green line, showing the up-up-down-down motif of Mn_A spins (red) along the crystallographic *a* axis. This originates the magnetic cell delimited with a black line and related to the crystallographic one via the transformation matrix: [(1 0 -1), (0 -1 0), (-2 0 0)] with an origin shift of (0, 0, 1/2) and magnetic space group P_c2_1/n (14.80). The ordering of the spins in Mn_2MnTeO_6 can be described as a 2D structure, where *ab* planes of interpenetrating Mn^{2+} AFM zig-zag chains are separated by diamagnetic TeO_6 octahedra. The spins are confined in the *ac* plane and stacked ferromagnetically along *b* (Mn–Mn interatomic distances of 5.429(1) Å). Both sublattices are AFM coupled among them via Mn_A-O-$Mn_B \approx 90º$ (see Table 1) superexchange pathways along [0 0 1] and [-1 0 1/2] directions of the crystallographic cell. These are the dominant interactions, schematised with red and blue lines and refined to 3.065(9) and 3.265(8) Å respectively, as labelled in Figure SF3c. FM Mn_A-Mn_B (3.395(8) Å) interactions occur via superexchange as shown in black in Figure SF3a. Next order AFM interactions emerge between Mn_A-Mn_B (3.529(9) Å) and Mn_A-Mn_A (3.87(1) Å) of parallel intra- and opposed inter-layer chains respectively (as shown in Figures SF3b and SF3c in green). The strongest interactions satisfy the Goodenough-Kanamori-Anderson rules, which predict AFM behaviour for d^5-d^5 interactions at 90º.[2]

Figure SF4 shows the different spin environments for the Te and Mn_A and Mn_B cations in the Mn_2MnTeO_6 double perovskite. Mn_A shows a Mn_B spins tetrahedral topology around. This explains why the direction is perpendicular to the *a* direction. Mn_B site with a diamagnetic B' cation forms an fcc frustrated lattice.

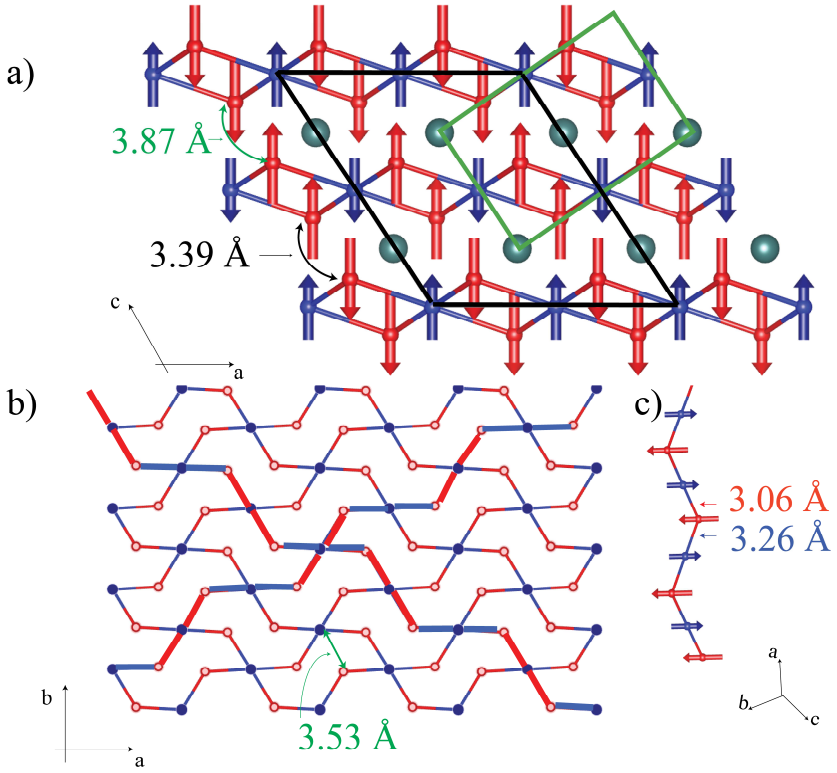

Figure SF3. a) *ac* plane of the magnetic structure of Mn_2MnTeO_6. Mn_A and Mn_B spins (red and blue arrows) describe AFM zig-zag chains via NN interactions (red and blue lines) into the *ab* plane. The green and black lines delimit the crystal and magnetic unit cells respectively. The nuclear unit cell is marked with a green line and the magnetic cell is delimited with a black line and related to the crystallographic one via the transformation matrix: [(1 0 -1), (0 -1 0), (-2 0 0)] with an origin shift of (0, 0, 1/2) and magnetic space group P_c2_1/n (14.80). b) *ab* Mn plane showing the interpenetration of chains running in opposed directions (two of them highlighted). c) section of a chain with Mn_A-Mn_B distances labelled, showing the dominant AFM interactions. Black and green bonds reflect next order FM and AFM interactions respectively, see the text.

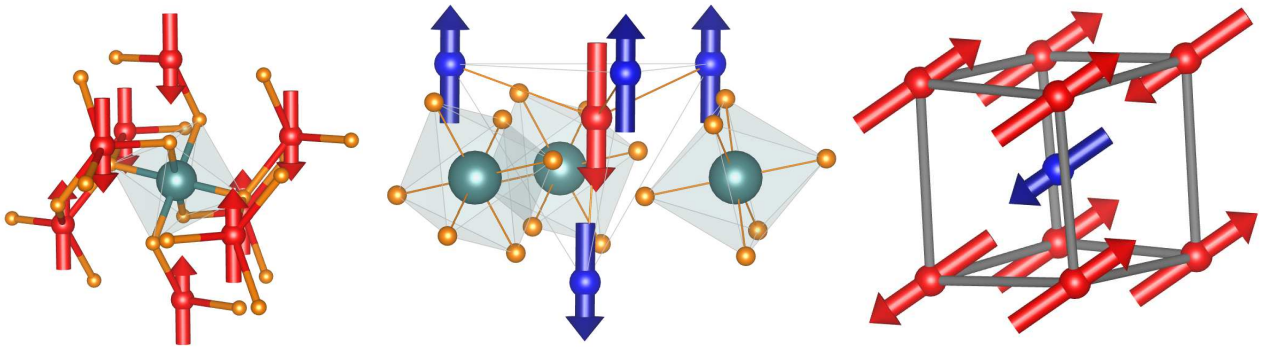

Figure SF4. Different spin topologies around Te, Mn_A and Mn_B cations (left, middle and right).

Supplementary Tables:

Table ST1. Irreducible representations (Irep) and basis vectors from the magnetic symmetry analysis of Mn_3TeO_6 with propagation vector [0.5 0 0.5]. The 4 symmetries and Ireps apply for 4e (Mn_A) site and only the two on the top half of the table of Ireps Γ_2 and Γ_4 are possible for 2b (Mn_B) site. Both magnetic sites follow Irep Γ_4. Independent contributions along *x* and *z* directions could be refined for both.

Irep / Symm	Γ_1			Γ_2			Γ_3			Γ_4		
x,y,z	100	010	001	100	010	001	100	010	001	100	010	001
-x+1/2,y+1/2,-z+1/2	-100	010	00-1	-100	010	00-1	100	0-10	001	100	0-10	001
-x,-y,-z	100	010	001	-100	0-10	00-1	100	010	001	-100	0-10	00-1
x+1/2,-y+1/2,z+1/2	-100	010	00-1	100	0-10	001	100	0-10	001	-100	010	00-1

Table ST2. Atomic positions determined from the Rietveld fit of 1.5 K NPD data. S.G. *P2₁/n*, *a* = 5.267(1) Å, b = 5.428(1) Å, *c* = 7.767(1) Å, *β* = 89.44(1) °.

Site	x	y	z	Biso	Occ	μ_x (μ_B)	μ_z (μ_B)*
Te (2a)	0	0	0	0.4 (5)	0.5		
Mn_B (2b)	0.5	0.5	0	0.03(67)	0.5	-3.6(1)	-1.8
Mn_A (4e)	0.489(3)	0.052(3)	0.234(2)	0.03(67)	1	4.2(1)	2.1
O1 (4e)	0.185(2)	0.293(2)	0.090(1)	0.4(3)	1		
O2 (4e)	0.695(2)	0.181(2)	-0.045(2)	0.4(3)	1		
O3 (4e)	0.875(2)	0.915(2)	0.219(1)	0.4(3)	1		

R_p = 6.6%, R_{wp} = 8.54%, R_f = 5.61%, R_B = 4.51%, R_{mag} = 10.4%, χ^2 = 1.23 %. * constrained to $\mu_x/2$

[1] J. Rodriguez-Carvajal, *Physica B*, 1993, **192**, 55.
[2] J.B. Goodenough, *Magnetism and the chemical bond.* Wiley, New York, 1963.